RESEARCH ARTICLE | MAY 20 2024

# Half bridge configurated magneto-resistive sensors with flux guide structure for enhancing sensitivity ⊕⊘

Suvechhya Lamichhane 💿 ; Yi Yang 💿 ; Andrei Sokolov 🗓 ; Xiaolu Yin; Yen-Fu Liu; Sy-Hwang Liou 🗷 👵



Appl. Phys. Lett. 124, 212401 (2024) https://doi.org/10.1063/5.0203392

A CHORUS





### Articles You May Be Interested In

Implementation of a full Wheatstone-bridge GMR sensor by utilizing spin—orbit torque induced magnetization switching in synthetic antiferromagnetic layer

J. Appl. Phys. (April 2023)

Linearization of the tunneling magnetoresistance sensors through a three-step annealing process

AIP Advances (January 2024)

Wheatstone bridge sensor composed of linear MgO magnetic tunnel junctions

J. Appl. Phys. (April 2010)





## Half bridge configurated magneto-resistive sensors with flux guide structure for enhancing sensitivity @

Cite as: Appl. Phys. Lett. 124, 212401 (2024); doi: 10.1063/5.0203392 Submitted: 13 February 2024 · Accepted: 5 May 2024 · Published Online: 20 May 2024











Suvechhya Lamichhane, 1 (b) Yi Yang, 1 (c) Andrei Sokolov, 2 (b) Xiaolu Yin, 1.2 Yen-Fu Liu, 1.2 and Sy-Hwang Liou 1.2.a) (b)



### **AFFILIATIONS**

#### **ABSTRACT**

We demonstrate the enhancement in sensitivity of half Wheatstone bridge configurated magneto-resistive sensors with a design of the magnetic flux guide. The efficacy of our flux guide design, in comparison to the conventional micro-magnetic flux concentrator for improving the flux gain, is studied using finite element method and verified with the experimental result. We observed a sensitivity of 260%/mT for our half Wheatstone bridge sensor with a very small coercivity of 0.01 mT at room temperature. Our work will contribute to paving a road map for mass production of sensitive magneto-resistive sensors with small footprints (2.5 mm<sup>2</sup> in this study).

Published under an exclusive license by AIP Publishing. https://doi.org/10.1063/5.0203392

Magnetic tunnel junction (MTJ) sensors, utilizing the tunneling magnetoresistance (TMR) effect, have displayed strong competitiveness across a wide array of applications, including current sensing, 1biosensing,<sup>4,5</sup> and defect testing.<sup>6,7</sup> Their exceptional performance can be attributed to their remarkable features, such as high sensitivity, spatial resolution, compact form factor, low power consumption, and seamless integration into chip systems.8-

In the presence of an external magnetic field, the resistance of MTJs undergoes variations depending upon the relative orientation of magnetization within the free layer (FL) and pinned layer (PL). This results in minimum resistance when the magnetizations are aligned in parallel and maximum resistance when they are in an antiparallel alignment. 11 To achieve a null voltage output in the absence of an external field and to stabilize the sensor's performance over a wide temperature range, MTJ sensors are typically structured in a full Wheatstone bridge configuration, where adjacent bridge arms must exhibit an antiparallel magnetization pinning. 12 Various studies have explored different strategies by taking two dies (there are two MTJ elements for each die) and rotating them so that the pinning directions were opposite to each other to create a full Wheatstone bridge. Additionally, local magnetic annealing techniques have been employed to align the pinning directions of the opposite bridge arms in the same orientation. 14-16 An alternative approach, suggested by different studies involves depositing distinct MTJ stacks with double or triple layers

of synthetic antiferromagnets on the same substrate, to attain this antiparallel pinning while subjecting them to the same magnetic annealing conditions. 17–19 Nevertheless, all of these methods present challenges when it comes to large-scale industrial production. As a simplification for production, the half bridge structure, comprising two sensitive arms and two reference arms, serves as a reliable alternative. The reference arms are created by shielding the sensor, and their purpose is to provide stability in the sensor against thermal shift to work in a large temperature range. 20,21 However, the output voltage for the half bridge sensor configuration is one half times of the output voltage for the full Wheatstone bridge where the sensitivity needs to be compromised.<sup>22</sup>

Recent research studies have been primarily focused on elevating the sensitivity of sensors through the utilization of magnetic flux concentrators (MFCs).<sup>23–25</sup> Numerical simulations have been employed to investigate the influence of MFC shapes and the spacing between them on magnetic flux amplification. 26,27 Additionally, various studies have experimentally implemented a double-layer MFC with distinct magnetic materials to achieve a substantial increase in sensitivity.<sup>2</sup> Furthermore, we have previously employed the approach of combining a micro-MFC with an external MFC to enhance the signal of the MTJ bridge.<sup>30</sup> However, all the efforts still are insufficient to incorporate the flux amplification in terms sensitivity gain in the sensor because there exists a gap between a pair of magnetic flux concentrators to accommodate sensing elements. When the width of this gap is

<sup>&</sup>lt;sup>1</sup>Department of Physics and Astronomy, University of Nebraska-Lincoln, Lincoln, Nebraska 68588, USA

 $<sup>^2</sup>$ Nebraska Center for Materials and Nanoscience, University of Nebraska-Lincoln, Lincoln, Nebraska 68588, USA

a) Author to whom correspondence should be addressed: sliou@unl.edu

significantly larger than the thickness of the magnetic flux concentrators, it results in a notable loss of magnetic flux density within the gap. <sup>26</sup> To mitigate this loss in flux density, our recent study demonstrates the use of a flux guide structure with an external MFC in a full Wheatstone bridge configuration. This approach has resulted in an impressive 2760-fold enhancement in sensitivity. <sup>31</sup>

In this study, we incorporate the flux guide structure to a half bridge configured magnetic tunnel junction (MTJ) sensor for enhancing the sensitivity. We designed the MTJ stack to incorporate the flux guide structure within the stack with a  $\sim \! 100$  nm thick, soft magnetic layer without compromising on the linearity of the sensor. The utilization of the flux guiding structure is expected to significantly boost the flux gain, especially at the central region where the free layer is located [Fig. 1(a)]. This enhancement facilitates the penetration of flux to reach the free layer, thereby amplifying the sensor's sensitivity. This improvement has been substantiated through both simulation and experimental findings, as discussed in this study.

The flux guide structure is a soft magnetic layer establishing a connection between laminated micro-MFCs. Additionally, we

conducted finite element method (FEM) simulations to investigate the flux gain in the flux guide by varying the thickness of the flux guide material.

We have a representation of the flux guide structure with MTJ cells depicted in Fig. 1(a) The MTJ cells are constructed as slender rectangles measuring  $5 \times 20 \,\mu\text{m}^2$ . To implement the flux guide structure in the sensor, we design our MTJ stacks as follows: The detailed layer structure is Si/SiO<sub>2</sub> (150)/Ta (2)/Ru (10)/Cu (2)/Ir<sub>20</sub>Mn<sub>80</sub> (6)/  $Co_{70.5}Fe_{4.5}Si_{15}B_{10}$  (50)/Cu (2)/ $Ir_{20}Mn_{80}$  (6)/ $Co_{70.5}Fe_{4.5}Si_{15}B_{10}$  (50)/Ru  $(0.5)/Co_{20}Fe_{60}B_{20}$  (3.4)/MgO (2)/Co<sub>20</sub>Fe<sub>60</sub>B<sub>20</sub> (4.5)/Ru (0.85)/Co<sub>40</sub>Fe<sub>60</sub> (3.5)/Ir<sub>20</sub>Mn<sub>80</sub> (10)/Ru (5)/Ta (5)/Ru (15), where the numbers in parentheses are thicknesses in nanometers, as shown in Fig. 1(b). It is noteworthy that the stack is designed with the free layer (FL) positioned at the bottom, featuring an additional soft magnetic layer of CoFeSiB, approximately 100 nm thick. This supplementary layer serves two purposes: enhancing the softness of the free layer through exchange coupling and serving as the flux guide. To create the flux guide, a substantial area of the free layer is preserved, and a 7.2  $\mu$ m thick pair of magnetic flux concentrator (MFC) structures, composed

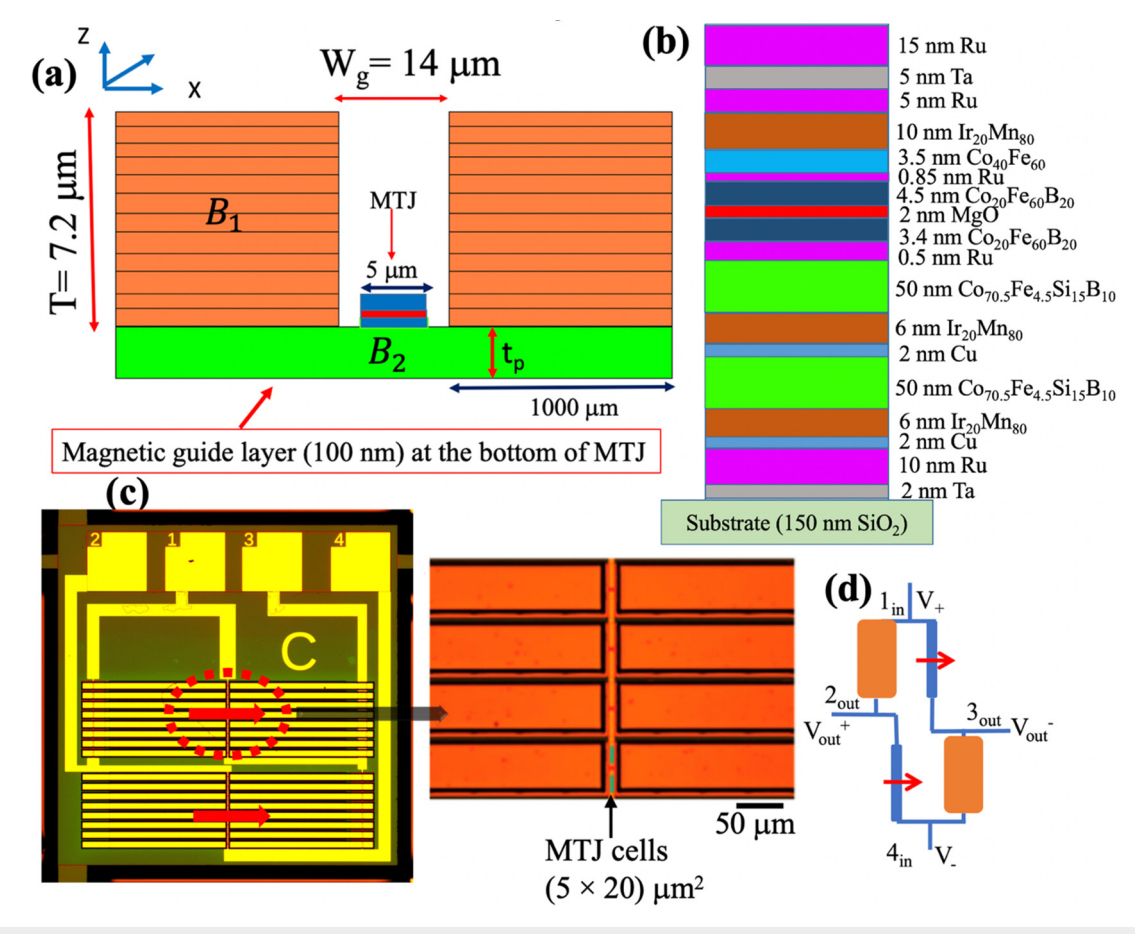


**FIG. 1.** (a) The schematics of the flux guide structure with the MTJ sensor showing the total thickness of laminated Conetic (T) as 7.2  $\mu$ m and the gap between Conetic (W<sub>g</sub>) as 14  $\mu$ m. The thickness of magnetic layer (t<sub>p</sub>) acting as a flux guide is 100 nm. (b) The MTJ stack deposited on the Si wafer, a detailed layer structure with the thickness is mentioned. (c) The optical image of the lithographically patterned MTJ device. The enlarged area shows the sensing arms of MTJ cells connected with the micro MFCs forming a flux guide. 16 MTJ junctions are connected in series in one sensing arm. (d) The MR sensor configurated in a half Wheatstone bridge. The reference arms are shielded by the MFCs.

of Conetic alloy (Ni<sub>77</sub>Fe<sub>14</sub>Cu<sub>5</sub>Mo<sub>4</sub>), is deposited as shown in Fig. 1(a). These two MFC structures are laminated with 65 layers where Conetic films of 100 nm are separated by copper of 10 nm to have a stack with a total thickness of 7.2  $\mu$ m. It has been shown that laminated magnetic films, despite having a total magnetic thickness of several micrometers, can have lower coercivity and saturation field compared to single-layer films with the same total magnetic thickness.<sup>32</sup> For improving the linearity of the sensor, we use the exchange bias in the free layer by incorporating 6 nm of IrMn which can be set orthogonal to the pinned layer where we used 10 nm of IrMn during the annealing.3 Photolithography and ion milling were used to transform the deposited film into MTJ devices. Figure 1(c) shows the lithographic pattern of the fabricated half Wheatstone bridge device with a zoomed view of the pattern of the soft magnetic layer and the magnetic tunnel junction cells, each measuring  $5 \times 20 \,\mu\text{m}^2$ . To establish the pinning direction of the pinned (reference) layer, the MTJ samples on the wafer underwent initial annealing in a magnetic field of 3 T at a constant temperature of 285 °C within a vacuum for 2 h. Figure 1(d) shows the terminal connection of the half Wheatstone bridge sensor.

We performed a FEM study to model the magnetic flux density within the flux guide magnetic layer and assess the magnetic amplification properties of our flux guide using FEMM software (see S1 in the supplementary material). The simulation encompassed a total length (L) of  $1000\,\mu\text{m}$ . The two laminated Conetic structures are connected by a soft magnetic material, with a combined thickness of laminated Conetics (T) of  $7.2\,\mu\text{m}$  and a separation gap width (Wg) of  $14\,\mu\text{m}$ , which is consistent with the parameter used in our physical fabrication. The thickness of the magnetic layer (tp) or flux guiding structure linking the two laminated Conetic structures was varied within the range of  $100\,\text{nm}$  to  $3\,\mu\text{m}$  during the simulation while experimentally we have  $100\,\text{nm}$  to the relative permeability of air to 1, and the soft

magnetic area was assigned a value of 1000. We defined the flux gain as the ratio of the magnetic flux density within the magnetic layer  $(B_2)$ to the magnetic flux density on the Conetic structure  $(B_1)$ , i.e.,  $B_2/B_1$ . Figure 2(a) shows the simulated flux flow in the conventional MFCs. Simulation results for the conventional flux concentrator indicate an enhancement in flux in the gap between the MFCs as compared with the flux density in the air. This enhancement is attributed to the saturation magnetization of the laminated concentrator ( $4\pi M_s$ ), which plays a significant role in this effect. Figure 2(b) shows the flux flow in the MFCs connected with the magnetic layer or flux guide of thickness  $1 \mu m$ . Clearly, we can see the significant enhancement of magnetic flux in the flux guide structure in comparison to the air gap. We plotted the flux gain corresponding to the thickness of the magnetic layer varying from 100 nm to 3  $\mu$ m as shown in Fig. 2(c). It becomes evident that a thinner magnetic layer width results in a significant enhancement of the flux gain across the structure. This observation aligns with the flux continuity model, which posits that due to the conservation of flux, a substantial portion of the flux must pass through the thin magnetic layer, resulting in flux gain

$$B_1TD=B_2t_pD,$$
 Flux Gain  $\left(rac{B_2}{B_1}
ight)=rac{T}{t_p}.$ 

This differs from the conventional magnetic flux concentrator, where flux is lost in the air gap.

The variation in flux gain at different positions for various thicknesses of the flux guide layer is shown in Fig. 2(d). However, at a thickness of 100 nm, the gain exhibits irregularities attributable to the leakage of the flux into the surrounding air as compared to the thicker magnetic layer. Additionally, the edges or boundaries of a magnetic material can disrupt the continuity of magnetic domains, leading to the formation of domain walls or changes in magnetization direction.

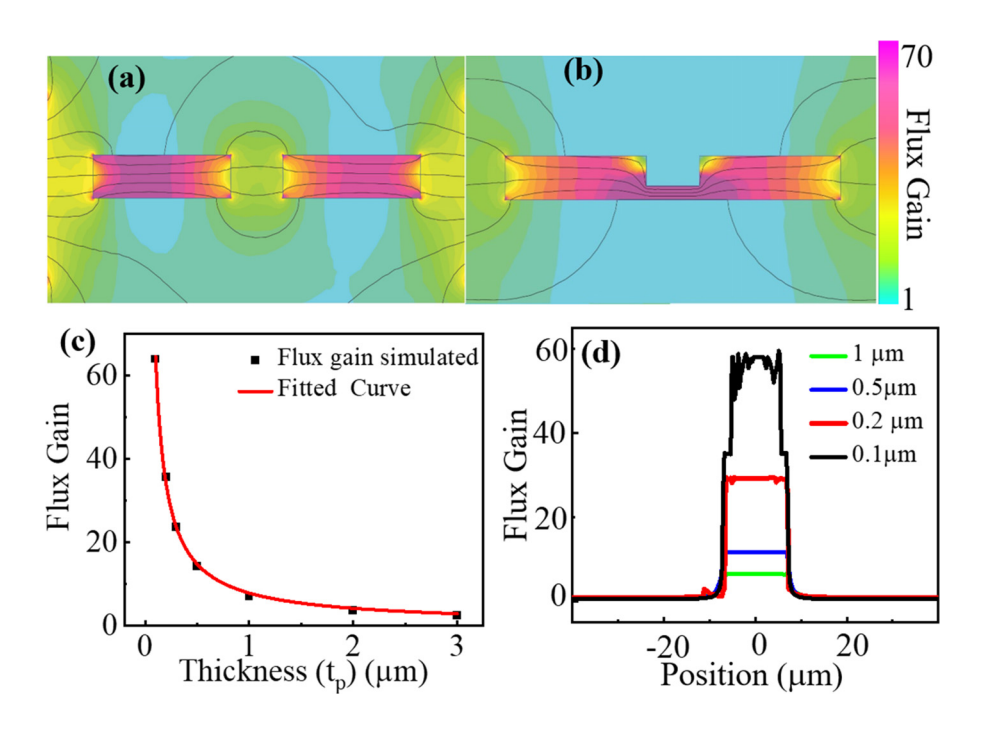


FIG. 2. (a) The flux flow simulated in the conventional MFCs with a gap of 14  $\mu$ m between them. (b) The flux flow in the flux guide structure with a magnetic layer of 1  $\mu$ m. The color bar shows the flux gain, i.e., ratio of flux in the gap to the flux in the MFCs. (c) Flux gain plotted against the thickness of the magnetic layer connecting the MFCs. The fitting is done with  $T/t_p$  which is the flux gain obtained from the flux continuity model, where T is  $7.2\,\mu$ m for our case. This shows the efficacy of the flux continuity model to explain the flux gain. (d) The horizontal line profile drawn shows the gain in the thin magnetic layer

This results in higher magnetic energy and increased reluctance to the flow of magnetic flux.  $^{37}$ 

The flux continuity model provides a reliable estimate of flux gain within the continuous system, except for cases involving very thin magnetic layers. According to our experimental findings, the flux guiding structure achieved a 52-fold flux gain for a 100 nm magnetic layer (which is very close to about 60-fold that is predicted from the model) used in fabrication, as demonstrated in Fig. 3 and discussed later in the text. Hence, the flux guide structure can be incorporated in the sensor to enhance the sensitivity and it holds great promise for the application in different types of sensors.

We conducted tunneling magnetoresistance (TMR) at room temperature in a zero-Gauss environment, with measurements conducted along the pinning direction (i.e., a magnetic field was applied along the pinning direction). For TMR, we applied  $0.1\,\mu\text{A}$  current using a Keithley 6221 source across terminals 1 and 4, simultaneously measuring voltage with a Keithley 2182 nanovoltmeter [Fig. S2(a) in the supplementary material]. Sensor performance was evaluated by applying voltage across terminals 1 and 4 via a 1.5-V battery, measuring resulting output voltage between terminals 2 and 3 [Fig. S2(b) in the supplementary material].

First, we assess the gain of the flux guide structure. We conducted the TMR measurement on the MTJ device before depositing the MFCs, as illustrated in Fig. 3(a). Following the deposition of the MFCs, we measured only the response of the one MTJ arm that has the MFC structure to estimate the gain from the flux guide. The TMR response for this specific configuration is presented in Fig. 3(b). The observed sharpness in the TMR response indicates an enhancement in

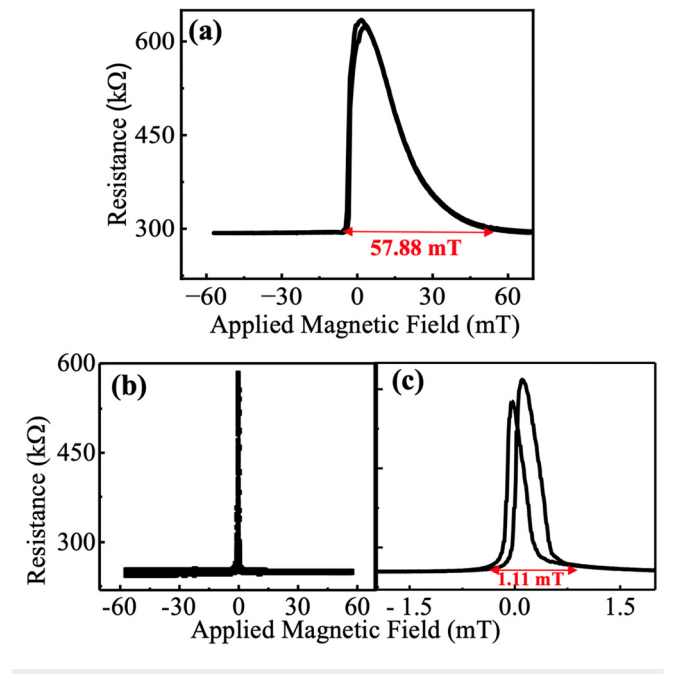


**FIG. 3.** (a) The TMR response of the MTJ devices before depositing the flux concentrator (Conetic layers). The TMR is approximately 110%. (b) To estimate the flux gain with our structure, we measure the TMR of the single arm after depositing the MFCs. (c) The TMR response in the small field range of -1.8 to +1.8 mT.

free layer (FL) performance due to the flux gain from the deposited flux concentrator. Figure 3(c) shows the TMR response from the small field range of -1.8 to +1.8 mT of the one MTJ arm. Clearly, our estimated gain in this context is approximately 52 times.

In Fig. 4, we show the magnetoresistance TMR response of the half Wheatstone bridge configured MTJ device (that includes the shielded and MTJ elements with MFCs) at room temperature.

Figure 4(a) presents the magnetoresistance data across a field range of -70 to +70 mT, which is a response from all four arms after the deposition of the flux concentrator. In this low-field regime (-2 to)+2 mT), the response of the reference arm, which is typically shielded and serves as a reference point for comparison, becomes negligible. This implies that the reference arm experiences minimal changes in resistance or response to the applied magnetic field within this narrow field range. However, when the external magnetic field exceeds ±20 mT, the shielding provided by the laminated Conetic (MFCs) material vanished. This leads to the penetration of the shielded region by the magnetic field, resulting in a response from all four arms of the TMR sensor. As shown in Fig. 4(b), there is a very large change in TMR in a narrower range of the magnetic field (-2 to +2 mT), hence, the effectiveness of the flux guide structure becomes more prominent. We further performed the TMR measurement by narrowing the magnetic field to demonstrate the very small coercive field of  $\sim$ 0.01 mT, as shown in Fig. 4(c).

The performance of the half bridge sensor is shown in Fig. 5. Figure 5(a) presents the output voltage of the sensor as measured within the field range from -60 to +60 mT, aligned with the pinned layer's pinning direction, also known as the sensing direction. Again, at high fields, the MFC gets saturated which leads to the penetration of the shielded region by the magnetic field, resulting in a response from

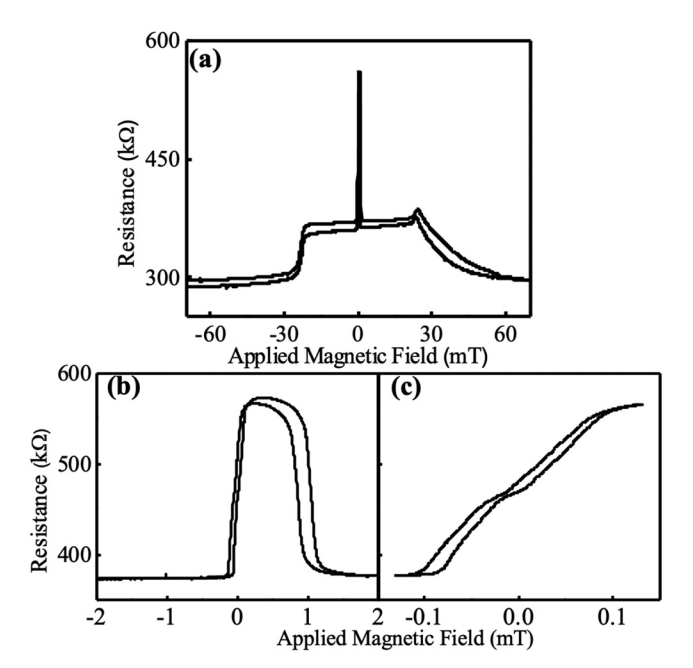


**FIG. 4.** (a) TMR response of the half Wheatstone bridge configured MTJ device at room temperature. (b) The TMR curve measured within a field range of  $\pm 2$  mT. (c) Small field range measurement for TMR showing a very small coercivity of 0.01 mT.

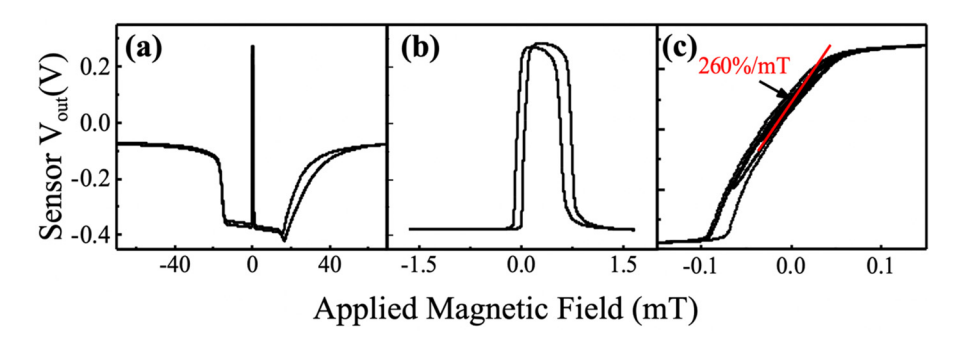
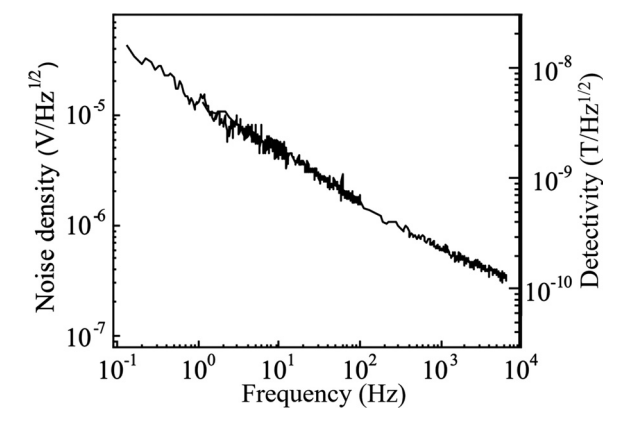


FIG. 5. (a) The output voltage of the sensor measured at room temperature, applying 1.5 V and a magnetic field along the pinning direction in the field range from -40 to +40 mT. The asymmetric response comes from the penetration of the field into the shielded arms. (b) The output voltage measured in a smaller field range from -1.5 to +1.5 mT. (c) The output voltage measured on the field range of -0.1 to +0.1 mT, for estimating sensitivity. From this small field range, we estimate the coercivity of 0.01 mT.

all four arms. In Fig. 5(b), we display the output voltage measured within a narrower field range, specifically from -2 to +2 mT. There are very large voltage changes in a small change magnetic field. This high sensitivity underscores the effectiveness of our innovative flux guiding structure. For the magnetic sensor, the minor loops are more interesting for practical applications, where only the magnetization of the free layer is switched while the pinned layer remains nearly unaffected. The minor loops were obtained by sweeping an external field of -0.1 to +0.1 mT, as shown in Fig. 5(c), which exhibits very small hysteresis and has a coercive field of less than 0.01 mT. Based on the data presented in Fig. 5(c), we estimated the slope  $\Delta V/\Delta H$  and employed the formula  $S = \frac{\Delta V_{out}/V_{in} \times 100^{10}}{\Delta H}$ , where the  $V_{in}$  is 1.5 Volt. We determined the sensor's sensitivity to be about 260%/mT (see the supplementary material, Sec. S2).

Furthermore, we conducted noise measurements following a methodology similar to our prior studies. <sup>11</sup> These measurements were conducted within a zero-Gauss chamber, with these half bridge sensors powered by a 1.5-V alkaline battery. We utilized a Model SR785 Dynamic Signal Analyzer to obtain the noise amplitude spectra. We have shown that the noise spectra remain unaffected with the deposition of MFCs as reported in our earlier studies. <sup>31</sup> Figure 6 depicts the



**FIG. 6.** Noise measurement of a half bridge configured sensor at room temperature plotted against frequency. The left axis is the noise spectra and the right axis is the corresponding detectivity estimated using the equation  $\frac{1}{S} \frac{\sqrt{S_V}}{V}$ .

noise spectra as well as the detectivity obtained under zero applied field conditions at room temperature. This measurement was performed in a zero-Gauss chamber. The detectivity was determined using the equation  $Detectivity = \frac{1}{S} \frac{\sqrt{S_V}}{V}$ . At a frequency of 10 Hz, the detectivity was found to be 1 nT/Hz<sup>1/2</sup>. The schematics and details of the noise measurement are presented in S3 of the supplementary material.

In summary, our comprehensive investigation of a magnetic flux guiding structure, conducted through simulations and experiments, aimed to enhance the sensitivity of magnetic tunnel junction-based magneto-resistive sensors. The results indicate that the half bridge MTJ device with the flux guide achieves a sensitivity of 260%/mT and a detectivity of  $1\ nT/Hz^{1/2}$  at  $10\ Hz$  rendering it suitable for applications requiring a highly sensitive magnetic field detection. Our study paves the way for the scalable production of MTJ sensors with enhanced sensitivity.

See the supplementary material for FEM simulation details (S1), TMR and sensor measurement (S2), and details of noise measurement (S3).

This research was supported by the National Science Foundation/EPSCoR RII Track-1: Emergent Quantum Materials and Technologies (EQUATE), Award No. OIA-2044049. This research was performed in part in the Nebraska Nanoscale Facility: the National Nanotechnology Coordinated Infrastructure and the Nebraska Center for Materials and Nanoscience, which are supported by the National Science Foundation under Award ECCS: 2025298, and the Nebraska Research Initiative.

# AUTHOR DECLARATIONS Conflict of Interest

The authors have no conflicts to disclose.

#### **Author Contributions**

Suvechhya Lamichhane: Conceptualization (equal); Formal analysis (equal); Investigation (equal); Software (equal); Writing – original draft (lead); Writing – review & editing (equal). Yi Yang: Conceptualization (equal); Investigation (supporting); Methodology (supporting); Validation (equal); Writing – review & editing (supporting). Andrei Sokolov: Formal analysis (equal); Investigation (equal); Validation

(supporting); Writing – review & editing (supporting). Xiaolu Yin: Conceptualization (equal); Methodology (equal); Validation (equal). Yen-Fu Liu: Conceptualization (equal); Methodology (equal); Validation (equal). Sy-Hwang Liou: Conceptualization (equal); Formal analysis (equal); Funding acquisition (lead); Supervision (lead); Validation (lead); Writing – review & editing (equal).

#### **DATA AVAILABILITY**

The data that support the findings of this study are available from the corresponding author upon reasonable request.

#### REFERENCES

- <sup>1</sup>K.-Z. Gao, X. Yin, Y. Yang, D. Ewing, P. J. De Rego, and S.-H. Liou, "MTJ based magnetic sensor for current measurement in grid," AIP Adv. **10**(1), 015301 (2020).
- <sup>2</sup>J. Sanchez Moreno, D. Ramirez, S. I. Ravelo Arias, P. Lopes, S. Cardoso, R. Ferreira, and P. Freitas, "Electrical characterization of a magnetic tunnel junction current sensor for industrial applications," IEEE Trans. Magn. 48, 2823–2826 (2012).
- <sup>3</sup>M. D. Cubells-Beltran, C. Reig, D. R. Munoz, S. I. P. C. de Freitas, and P. J. P. de Freitas, "Full wheatstone bridge spin-valve based sensors for IC currents monitoring," IEEE Sens. J. 9(12), 1756–1762 (2009).
- <sup>4</sup>C. Ghemes, O.-G. Dragos-Pinzaru, M. Tibu, M. Lostun, N. Lupu, and H. Chiriac, "Tunnel magnetoresistance-based sensor for biomedical application: Proof-of-concept," Coatings 13(2), 227 (2023).
- <sup>5</sup>A. Kanno, N. Nakasato, M. Oogane, K. Fujiwara, T. Nakano, T. Arimoto, H. Matsuzaki, and Y. Ando, "Scalp attached tangential magnetoencephalography using tunnel magneto-resistive sensors," Sci. Rep. 12(1), 6106 (2022).
- <sup>6</sup>Z. Jin, M. A. I. Mohd Noor Sam, M. Oogane, and Y. Ando, "Serial MTJ-based TMR sensors in bridge configuration for detection of fractured steel bar in magnetic flux leakage testing," Sensors 21(2), 668 (2021).
- <sup>7</sup>D. W. Guo, F. A. Cardoso, R. Ferreira, E. Paz, S. Cardoso, and P. P. Freitas, "MgO-based magnetic tunnel junction sensors array for non-destructive testing applications," J. Appl. Phys. 115(17), 17E513 (2014).
- <sup>8</sup>B. Lim, M. Mahfoud, P. T. Das, T. Jeon, C. Jeon, M. Kim, T.-K. Nguyen, Q.-H. Tran, F. Terki, and C. Kim, "Advances and key technologies in magnetoresistive sensors with high thermal stabilities and low field detectivities," APL Mater. 10(5), 051108 (2022).
- <sup>9</sup>S. Yan, Z. Zhou, Y. Yang, Q. Leng, and W. Zhao, "Developments and applications of tunneling magnetoresistance sensors," Tsinghua Sci. Technol. 27(3), 443–454 (2022).
- 10 C. Zheng, K. Zhu, S. Cardoso de Freitas, J.-Y. Chang, J. E. Davies, P. Eames, P. P. Freitas, O. Kazakova, C. Kim, C.-W. Leung, S.-H. Liou, A. Ognev, S. N. Piramanayagam, P. Ripka, A. Samardak, K.-H. Shin, S.-Y. Tong, M.-J. Tung, S. X. Wang, S. Xue, X. Yin, and P. W. T. Pong, "Magnetoresistive sensor development roadmap (non-recording applications)," IEEE Trans. Magn. 55(4), 1–30 (2019).
- <sup>1</sup>S. H. Liou, X. Yin, S. E. Russek, R. Heindl, F. C. S. Da Silva, J. Moreland, D. P. Pappas, L. Yuan, and J. Shen, "Picotesla magnetic sensors for low-frequency applications," IEEE Trans. Magn. 47(10), 3740–3743 (2011).
- <sup>12</sup>C. Reig, M. D. Cubells-Beltran, D. Ramirez, S. Cardoso, and P. P. Freitas, "Electrical isolators based on tunneling magnetoresistance technology," IEEE Trans. Magn. 44(11), 4011–4014 (2008).
- <sup>13</sup>P. P. Freitas, R. Ferreira, and S. Cardoso, "Spintronic sensors," Proc. IEEE 104(10), 1894–1918 (2016).
- <sup>14</sup>O. Ueberschar, M. J. Almeida, P. Matthes, M. Muller, R. Ecke, R. Ruckriem, J. Schuster, H. Exner, and S. E. Schulz, "Optimized monolithic 2-D spin-valve sensor for high-sensitivity compass applications," IEEE Trans. Magn. 51(1), 4002404 (2015).
- 15I. Berthold, M. Müller, S. Klötzer, R. Ebert, S. Thomas, P. Matthes, M. Albrecht, and H. Exner, "Investigation of selective realignment of the preferred magnetic direction in spin-valve layer stacks using laser radiation," Appl. Surf. Sci. 302, 159–162 (2014).

- <sup>16</sup>J. Cao and P. P. Freitas, "Wheatstone bridge sensor composed of linear MgO magnetic tunnel junctions," J. Appl. Phys. 107(9), 09E712 (2010).
- 17 R. Ferreira, E. Paz, P. P. Freitas, J. Ribeiro, J. Germano, and L. Sousa, "2-axis magnetometers based on full wheatstone bridges incorporating magnetic tunnel junctions connected in series," IEEE Trans. Magn. 48(11), 4107 (2012).
- <sup>18</sup>F. Franco, M. Silva, S. Cardoso, and P. P. Freitas, "Optimization of asymmetric reference structures through non-evenly layered synthetic antiferromagnet for full bridge magnetic sensors based on CoFeB/MgO/CoFeB," Appl. Phys. Lett. 118(7), 072401 (2021).
- <sup>19</sup>V. S. Luong, A. T. Nguyen, and T. H. D. Tran, "Antiparallel-pinned spin valves with modified artificial antiferromagnetic layer for full-bridge magnetic sensors," IEEE Trans. Magn. 54(11), 4001705 (2018).
- 20 T. Poon, N. Tse, and R. Lau, "Extending the GMR current measurement range with a counteracting magnetic field," Sensors 13, 8042–8059 (2013).
- <sup>21</sup>Z. Qian, D. Wang, J. M. Daughton, M. Tondra, C. Nordman, and A. Popple, "Linear spin-valve bridge sensing devices," IEEE Trans. Magn. 40(4), 2643–2645 (2004).
- $^{\bf 22}$  J. Daughton, "Spin-dependent sensors," Proc. IEEE  $\bf 91 (5), 681-686$  (2003).
- <sup>23</sup>K. Zhu and P. W. T. Pong, "Curved trapezoidal magnetic flux concentrator design for current measurement of multi-core power cable with magnetic sensing," IEEE Trans. Magn. 55(4), 4001809 (2019).
- <sup>24</sup>P. D. Kulkarni, H. Iwasaki, and T. Nakatani, "The effect of geometrical overlap between giant magnetoresistance sensor and magnetic flux concentrators: A novel comb-shaped sensor for improved sensitivity," Sensors 22(23), 9385 (2022).
- <sup>25</sup>P. Li, L. Pan, Y. Hu, Y. Che, J. Hu, M. Pan, Q. Du, Y. Yu, K. Sun, and X. Zhang, "A three-dimensional magnetic flux guide for magnetic tunnel junction sensors," IEEE Trans. Magn. 58(5), 4001905 (2022).
- <sup>26</sup>X. Sun, L. Jiang, and P. W. T. Pong, "Magnetic flux concentration at micrometer scale," Microelectron. Eng. 111, 77–81 (2013).
- <sup>27</sup>X. Zhang, Y. Bi, G. Chen, J. Liu, J. Li, K. Feng, C. Lv, and W. Wang, "Influence of size parameters and magnetic field intensity upon the amplification characteristics of magnetic flux concentrators," AIP Adv. 8(12), 125222 (2018).
- <sup>28</sup>J. Hu, M. Ji, W. Qiu, L. Pan, P. Li, J. Peng, Y. Hu, H. Liu, and M. Pan, "Double-gap magnetic flux concentrator design for high-sensitivity magnetic tunnel junction sensors," Sensors 19(20), 4475 (2019).
- <sup>29</sup>J. Valadeiro, D. C. Leitao, S. Cardoso, and P. P. Freitas, "Improved efficiency of tapered magnetic flux concentrators with double-layer architecture," IEEE Trans. Magn. 53(11), 4003805 (2017).
- 30 X. Yin, Y.-F. Liu, D. Ewing, C. K. Ruder, P. J. D. Rego, A. S. Edelstein, and S.-H. Liou, "Tuning magnetic nanostructures and flux concentrators for magnetoresistive sensors," in *Spintronics VIII* (SPIE, 2015), Vol. 9551, pp 144–153.
- <sup>31</sup>Y. Yang, A. Sokolov, X. Yin, J. Hua, Y.-F. Liu, S. Lamichhane, and S.-H. Liou, "Novel magnetic flux guiding structure of magnetoresistive sensor for increased sensitivity," IEEE Trans. Magn. 59(1), 4400107 (2023).
- <sup>32</sup>Y. Yang and S.-H. Liou, "Laminated magnetic film for micro magnetic flux concentrators," AIP Adv. 11(3), 035004 (2021).
- <sup>53</sup>G. Anderson, Y. Huai, and L. Miloslawsky, "CoFe/IrMn exchange biased top, bottom, and dual spin valves," J. Appl. Phys 87(9), 6989–6991 (2000).
- 34J. Nogués and I. K. Schuller, "Exchange bias," J. Magn. Magn. Mater 192(2), 203-232 (1999).
- 35L. Lombard, E. Gapihan, R. C. Sousa, Y. Dahmane, Y. Conraux, C. Portemont, C. Ducruet, C. Papusoi, I. L. Prejbeanu, J. P. Nozières, B. Dieny, and A. Schuhl, "IrMn and FeMn Blocking temperature dependence on heating pulse width,"
- J. Appl. Phys **107**(9), 09D728 (2010).

  <sup>36</sup>See https://scholar.google.com/citations?view\_op=view\_citation&hl=en&user
  =ExvMNWoAAAAJ&citation\_for\_view=ExvMNWoAAAAJ:Zph67rFs4hoC
  for "FEMM 4.2;" accessed 18 April 2023.
- 37 R. C. O'Handley, Modern Magnetic Materials (Wiley, 1999).
- <sup>38</sup>W. F. Egelhoff, P. W. T. Pong, J. Unguris, R. D. McMichael, E. R. Nowak, A. S. Edelstein, J. E. Burnette, and G. A. Fischer, "Critical challenges for picoTesla magnetic-tunnel-junction sensors," Sens. Actuators, A 155(2), 217–225 (2009).
- 39W. Zhao, X. Tao, C. Ye, and Y. Tao, "Tunnel magnetoresistance sensor with AC modulation and impedance compensation for ultra-weak magnetic field measurement," Sensors 22(3), 1021 (2022).